Naoki Fukuda
e-mail: fnaoki@tokyo-gas.co.jp

Hiroshi Yatabe

Shinobu Kawaguchi

Takahito Watanabe

Tomoki Masuda

Pipeline Engineering Research Laboratory,
Tokyo Gas Co., Ltd.,
1-7-7, Suehiro-cho, Tsurumi-ku,
Yokohama, 230-0045, Japan

Experimental and Analytical Study of Cold Bending Process for Pipelines

The behavior during the cold bending of pipelines was experimentally and analytically investigated. Full-scale cold bending experiments were performed on API X60 and X80 grade line pipes. Finite element (FE) analyses simulated the cold bending process by considering the contact interactions between a pipe and the components of the bending machine. The results of the simulation were in good agreement with the full-scale experiments. The stress-strain relationship and yield to tensile ratio (Y/T) had no obvious effect on the strain distribution after cold bending. The tensile tests quantitatively evaluated the decrease in the yield stress along the longitudinal direction on the cold bends due to the Bauschinger effect. [DOI: 10.1115/1.1554701]

1 Introduction

Cold field bending is widely used for bends having a large radius and a small bending angle in gas pipelines. Cold bends are made from straight pipes using a cold-forming process with a bending machine in the field. The cold bending process generally causes residual strain in the longitudinal direction of the pipes. The mechanical properties of the cold bends would then be different from the straight pipes due to work hardening and the Bauschinger effect [1].

For buried pipelines in the field, stress is generally introduced along their longitudinal direction by ground movements such as ground subsidence, lateral ground displacement, and landslides [2,3]. In addition, in areas where earthquakes frequently occur such as in Japan, seismic motion needs to be considered when designing pipelines [4,5]. Therefore, when using cold bends in these areas, the longitudinal strain distribution and the longitudinal mechanical properties should be quantitatively evaluated.

Although some studies have been conducted for local buckling by cold bending [6] and for the application of cold bending for large diameter pipes [7], the strain distribution after bending and the mechanical properties of cold bends have been hardly reported. The objective of this study is to investigate the longitudinal strain distribution of cold bends and the decrease in the longitudinal yield stress due to cold bending.

In order to clarify the longitudinal strain in pipes after cold bending, finite element (FE) analyses and experiments were performed. For the bending process simulation, the contacts between a pipe and the bending machine were taken into account. The simulation method was then verified by the results of the full-scale bending experiments with two series of line pipes. The longitudinal strain distribution, bending angle and change in diameter were measured in the experiments. The changes in the longitudinal mechanical properties of the cold bends were evaluated using the tensile tests.

2 Experiments and Analyses

2.1 Experiments

2.1.1 Materials. Full-scale bending experiments were performed on two series of UOE line pipes. Pipe A was API 5L X60 grade and Pipe B was X80 [8]. Table 1 shows the outer diameter and the wall thickness of the pipes. Table 2 summarizes the chemical compositions. The tensile tests were conducted in accordance with Japanese Industrial Standard (JIS) Z 2201 [9]. The tensile specimens were machined from the pipes along the longitudinal direction. Figure 1 illustrates a tensile specimen with a thickness of 12 mm. Figure 2 shows the stress-strain curves of Pipes A and B. Table 3 summarizes the mechanical properties of the pipes in the longitudinal direction. In Table 3, the yield stress denotes the stress at a 0.5% nominal strain. Table 3 and Fig. 2 indicate that the Y/T and the stress-strain relationship of Pipe A were obviously different from those of Pipe B.

2.1.2 Cold Bending. CRC-Evans PB12-16 and PB22-36 type bending machines were used for Pipes A and B, respectively. Figure 3 illustrates the structure of the bending machines. The bending machine is composed of a pin-up shoe, a die and a stiff back. The die is fixed to the bending machine, and oil cylinders move the pin-up shoe and the stiff back. Table 4 summarizes the dimensions of the bending machines. Dimensions *a*, *b*, *c*, *d*, and *R* were defined as shown in Fig. 3.

A mandrel, which prevents flattening deformation, is inserted inside the pipe on the stiff back before cold bending. The mandrel center is positioned at the die center. In the bending process, (1) the pipe and the pin-up shoe contact each other by lifting the pin-up shoe. (2) By lifting the stiff back, the pipe contacts the die. (3) The pipe is cold bent by tilting the stiff back.

The bending angle is controlled by the vertical displacement of cylinder C. The bending angle is generally defined as that measured at both edges of the pipe in an unloaded condition after bending. In this study, the bending angle was approximately 1 degree.

The location where the pipe contacts the die center is defined as the bending location. The location of the circumferential direction, α, is defined as 0 degree at the top where the compressive strain is generated, and 180 degrees at the bottom where the tensile strain is generated by the bending.

2.1.3 Measurements.

(1) Residual Strain and Bending Angle

The longitudinal strain and bending angles were measured before and after bending. The local strains were measured using strain gauges, and are expressed as positive if it is tensile and negative if compressive. The strain gauges were longitudinally attached at the $\alpha = 0$ degree location for intervals of 50 mm or 100 mm. Figure 4 shows the strain gauges attached to a pipe. The coating on the pipes was partly stripped for attachment of the strain gauges, and then recoated with resin.

Presented at the 20th International OMAE Conference, Rio de Janeiro, Brazil, June 3–18, 2001, of THE AMERICAN SOCIETY OF MECHANICAL ENGINEERS, and contributed by the OOAE Division for publication in the JOURNAL OF OFFSHORE MECHANICS AND ARCTIC ENGINEERING. Manuscript received July 2001; final revision, March 2002. Associate Editor: J. E. Indacochea.

Table 1 Dimensions of pipes

Pipe	Grade	Outer Diameter (mm)	Wall thickness (mm)	D/t
A	X60	407.2	13.2	30.8
B	X80	610.3	15.4	39.6

Table 2 Chemical compositions of pipes (wt%)

Pipe	Grade	C	Si	Mn	P	S
A	X60	0.08	0.25	1.50	0.013	0.002
B	X80	0.06	0.24	1.76	0.007	0.002

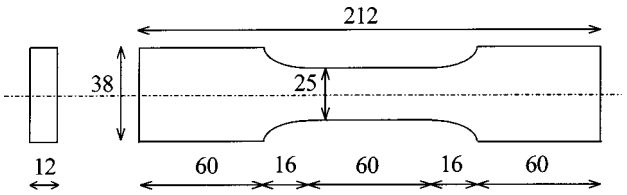

Fig. 1 Tensile specimen (mm)

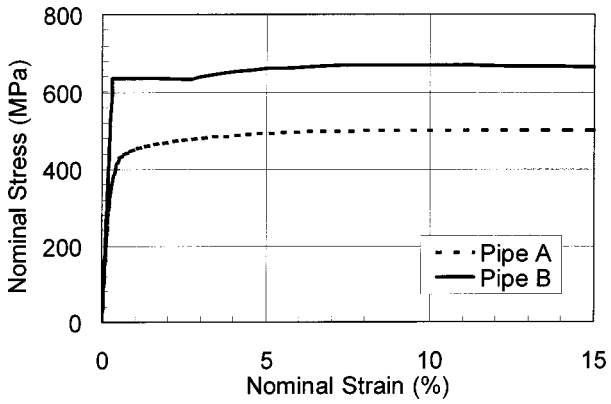

Fig. 2 Stress-strain curves

Table 3 Mechanical properties of pipes in the longitudinal direction

Pipe	Grade	Yield stress (MPa)	Tensile strength (MPa)	Y/T
A	X60	423	502	0.84
B	X80	633	670	0.94

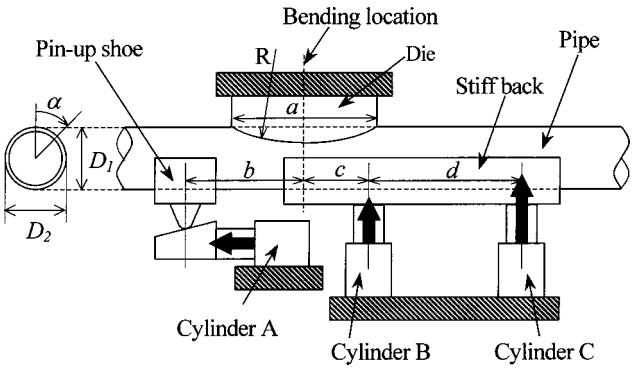

Fig. 3 Schematic structure of the bending machine (CRC-Evans type)

Table 4 Dimensions of bending machines

Pipe	Bending machine	Dimensions (mm) a	b	c	d	R
A	PB12-16	910	910	635	1220	12192
B	PB22-36	1625	1780	680	2760	18288

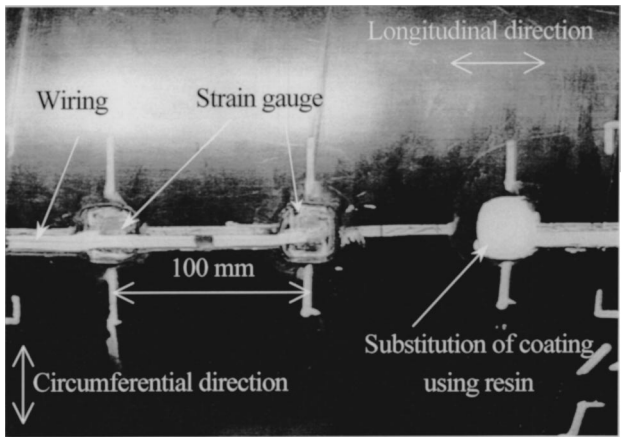

Fig. 4 External appearance of pipe and strain gauges before bending (Pipe A, $\alpha=0$ degree location)

(2) Ovality

The ovality, ξ, of the pipes was measured at the bending location after bending. ξ was calculated using Eq. (1):

$$\xi=(D_2-D_1)/D_s \quad (1)$$

D_1: Outer diameter along the perpendicular direction (Fig. 3).

D_2: Outer diameter along the horizontal direction (Fig. 3).

D_s: Nominal outer diameter (406.4 mm for Pipe A, 609.6 mm for Pipe B).

(3) Mechanical Properties

For a quantitative evaluation of the changes in the mechanical properties of the pipes due to the Bauschinger effect, tensile tests were performed for the cold bends. JIS Z2201 tensile specimens (Fig. 1) were machined from the cold bends along the longitudinal direction at the $\alpha=0$ degree location for Pipes A and B. The center of the tensile specimens was located at the maximum absolute value of the residual strain in the cold bends.

2.2 Simulation of Cold Bending Process

2.2.1 Finite Element Model. The cold bending process was simulated using the finite element (FE) method. Figure 5 shows an FE model for Pipe B. The pipe, the pin-up shoe, the die and the stiff back were modeled using finite elements; for the pin-up shoe, the die and the stiff back, 8-node solid elements were used, and for the pipes, 4-node shell elements. Due to the geometric and loading symmetries, only half of the pipe and the components of the bending machine were modeled. The outer diameter and the wall thickness used for the finite element modeling are presented in Table 1.

A Young's modulus of 205.8 GPa and a Poisson's ratio of 0.3 for the steel were used for the analyses. The yielding condition in the analyses followed the von-Mises yield criterion for isotropic hardening. The stress-strain curves presented in Fig. 2 were taken into account for the nonlinear finite element analyses.

The nonlinear deformations of the pipes were simulated. The contact interactions were defined with a small sliding option between the pipe and the die, and also between the pipe and the stiff

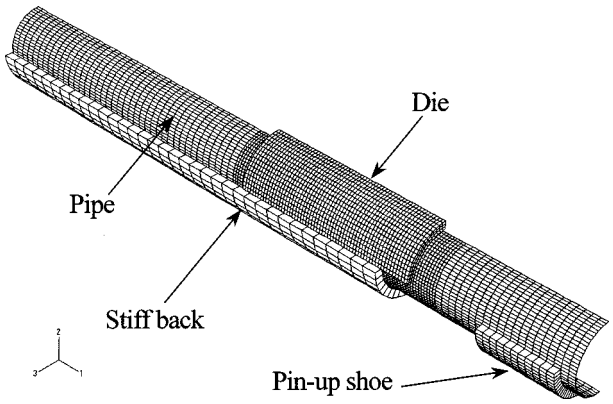

Fig. 5 Finite element model (Pipe B)

back. To simplify the model, the pin-up shoe was tied to the pipe. The contact between the mandrel and the pipe was modeled using nonlinear spring elements. ABAQUS Version 5.8 [10] was used as a solver for the analyses with geometric nonlinearity and large strain formulation.

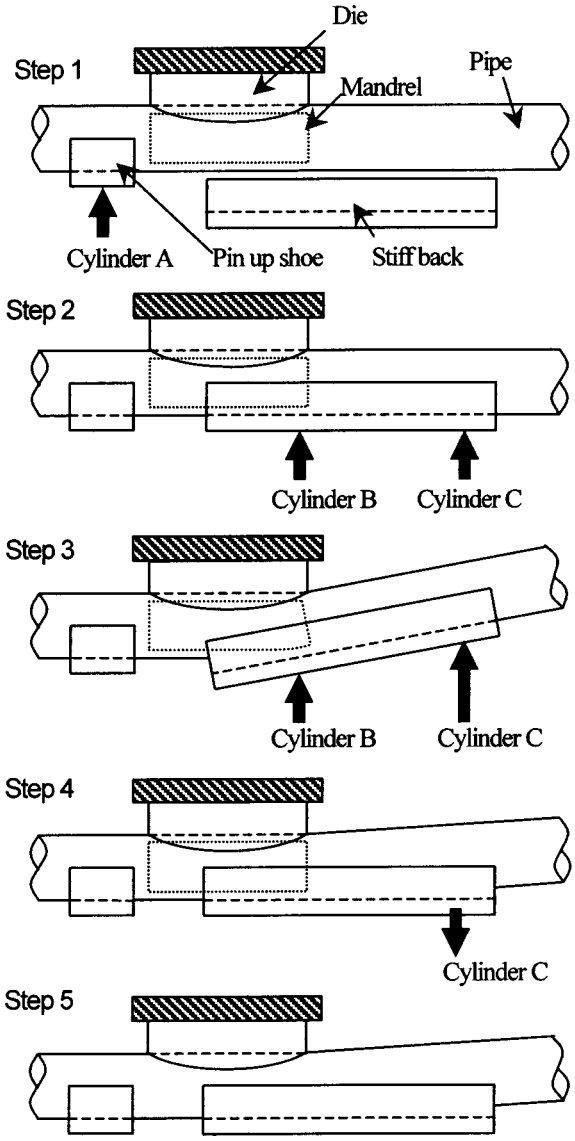

Fig. 6 Schematic diagram of cold bending process during FE analyses

Table 5 Operations of bending process during FE analyses

Step	Operations at each step
1	Move the pin-up upward and bring the pin-up into contact with the pipe.
2	Keep the stiff back horizontal and move it upward. Bring the stiff back into contact with the pipe.
3	Bend by tilting the stiff back: fix Cylinder B and move Cylinder C upward.
4	Unload by moving Cylinder C downward.
5	Remove the mandrel

Table 6 Boundary conditions for each step of FE analyses

		Displacement		
Step	Cylinder	Vertical	Horizontal	Rotation
1	A	Upward	Fix	Free
2	B, C	Upward	Fix	Free
3	B	Fix	Fix	Free
	C	Upward	Free	Free
4	C	Downward	Free	Free

2.2.2 Boundary Conditions. The cold bending process was divided into five steps as shown in Fig. 6 and Table 5. Displacement boundary conditions were applied at the nodes where the components of the bending machine and the cylinders contact each other. Table 6 summarizes the details of the boundary conditions in each step.

3 Results and Discussion

3.1 Residual Strain Distribution. Figures 7 and 8 show the residual strain distribution along the longitudinal direction at the $\alpha = 0$ degree location for Pipes A and B, respectively. In these figures, the lines and plots represent the results of the analyses and the experiments, respectively. The details of the analytical results are described in Section 3.3.

At the bending angle of 1 degree, the ranges of the compressive residual strain over 0.2% were approximately 400 mm and 600 mm for Pipes A and B, respectively. Under the present experimental conditions, the ranges were almost equal to the outer diameter of each pipe. In general, the actual original pipes are multiply bent in the field at an interval of the outer diameter. The present results indicated that the residual strain distribution does not overlap each other when each bending angle was 1 degree.

The maximum values of the compressive residual strain were 1.20% and 1.35% for Pipes A and B, respectively; the maximum

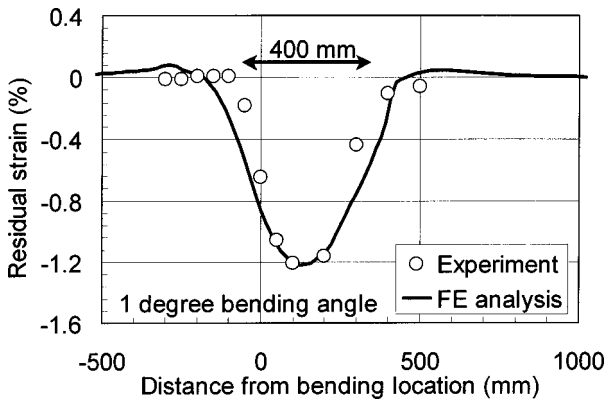

Fig. 7 Distribution of residual strain along the longitudinal direction (Pipe A)

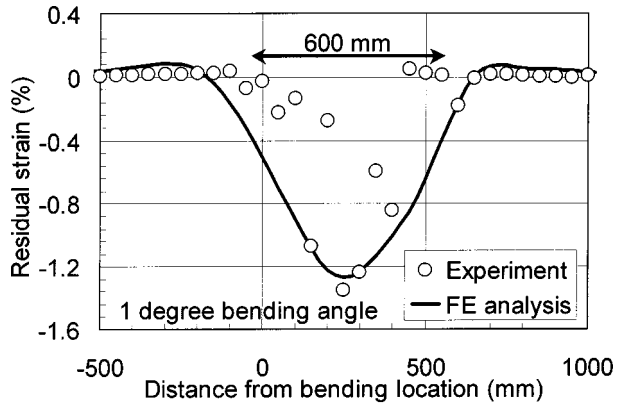

Fig. 8 Distribution of residual strain along the longitudinal direction (Pipe B)

values of both pipes were in good agreement with each other. The locations where the maximum value of the compressive residual strain was observed shifted +100 mm and +250 mm from the bending location for Pipes A and B, respectively. Due to the asymmetry of the bending machine, the behavior of the cold bending process differed from symmetrical three-point bending.

Table 7 Comparison of mechanical properties before and after bending

Pipe	Before or After bending	Maximum residual strain (%)	Yield stress (MPa)	Tensile strength (MPa)
A	Before	0	465	527
	After	−1.20	437	529
B	Before	0	633	670
	After	−1.35	461	656

3.2 Mechanical Properties in the Longitudinal Direction After Bending. Table 7 summarizes the results of the tensile tests for Pipes A and B before and after bending. The cold bending process reduced the yield stress of both pipes; the reduction in the yield stress was 6% and 27% for Pipes A and B, respectively. The decrease in the yield stress for Pipe B was greater than that for Pipe A. This indicated that the Bauschinger effect was more predominant for the higher strength (grade) and higher Y/T Pipe B than Pipe A.

3.3 Verification of the Simulation Method. Figures 9 and 10 illustrate the analytical results of the longitudinal strain distribution after bending for Pipes A and B, respectively. In these figures, the deformation magnification of both figures is one. The black and white parts represent the compressive and tensile strains, respectively. The arrows show the die center, that is, the bending location.

As described in Section 3.1, the location of the maximum compressive residual strain differed from the bending location in Figs. 7 and 8. This trend corresponded to the analytical results shown in Figs. 9 and 10. In addition, Figs. 7 and 8 show that the ranges of the residual strain in the analyses are in good agreement with the experimental results. Table 8 summarizes the experimental and analytical results of the bending angle, the maximum absolute value of the residual strain and the ovality. Good agreement was observed between the analyses and the experiments. In particular, the bending angle was predicted with high precision by the analyses. We concluded that the cold bending process for high-grade line pipes was predictable by the present simulation method.

3.4 Effect of Stress-Strain Relationship and Y/T on the Strain Distribution. Figures 11 and 12 show the changes in the strain distribution at the $\alpha=0$ degree location from the beginning to the end of Step 3 for Pipes A and B, respectively. In these figures, the distance from the bending location and the displacement of Cylinder C were normalized by the nominal outer diameter (406.4 mm for Pipe A, 609.6 mm for Pipe B) and the maximum displacement of Cylinder C, respectively. In these figures, δ

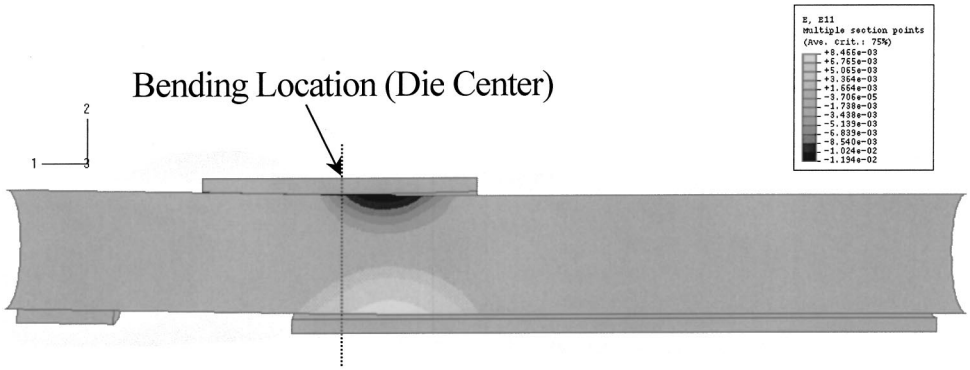

Fig. 9 Deformation and distribution of strain after bending process (Pipe A)

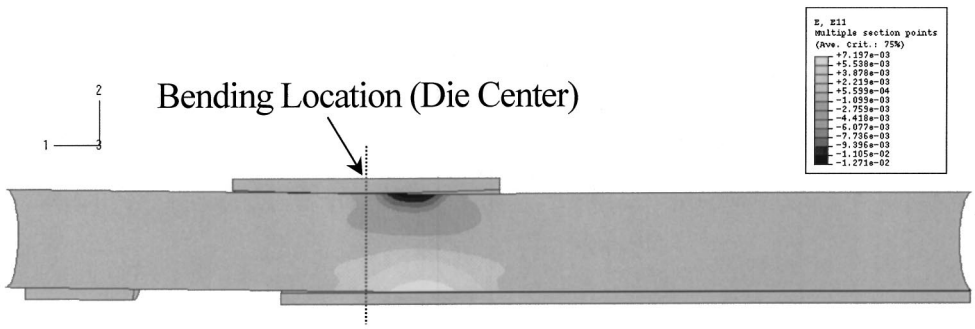

Fig. 10 Deformation and distribution of strain after bending process (Pipe B)

Table 8 Summary of experiments and FE analyses

	Pipe	Experiments (a)	Analyses (b)	Difference $\lvert(a)-(b)\rvert$
Bending angle (degrees)	A	0.98	1.11	0.13
	B	0.93	0.92	0.01
Maximum residual strain (%)	A	−1.20	−1.22	0.02
	B	−1.35	−1.27	0.08
Ovality (%)	A	1.67	1.14	0.53
	B	0.77	0.71	0.06

represents the normalized displacement of Cylinder C. $\delta=0$ at the beginning of Step 3 and $\delta=1$ at the end of Step 3.

The stress-strain relationship around a 1% strain in Fig. 1 shows that Pipes A and B differ in their yield; Pipe B has a yield plateau. In addition, Table 3 shows that the Y/T values of both pipes are obviously different. However, Figures 11 and 12 illustrated that the longitudinal strain distribution is similar for Pipes A and B. This indicated that the stress-strain relationship and Y/T have no obvious effects on strain distribution due to cold bending.

If the cold bending process is load-dominant bending deformation, the local deformation and strain concentrations should be observed for Pipe B. However, this behavior was not observed in Figures 10 and 12 for Pipe B. Based on this fact, it was inferred that the cold bending process is a displacement-dominant deformation.

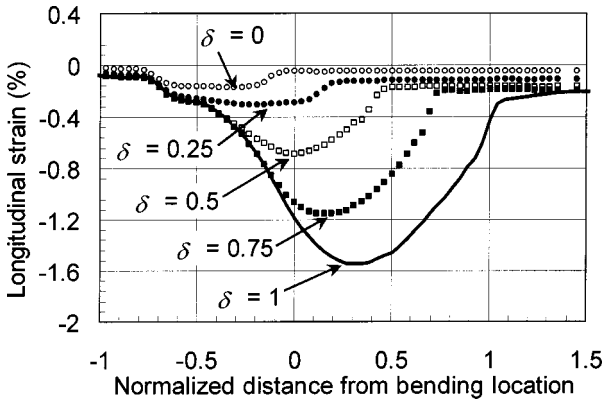

Fig. 11 Change in strain distribution (Pipe A)

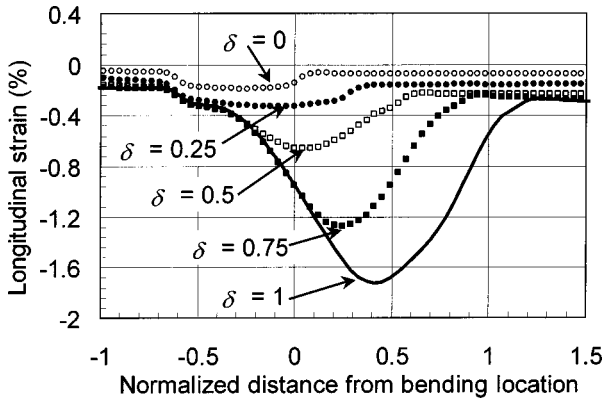

Fig. 12 Change in strain distribution (Pipe B)

4 Conclusions

1. The FE analyses method was established for simulating the cold bending process by considering the contact interaction between a pipe and the components of the bending machine for high-grade line pipe.
2. The results of the FE analyses were in good agreement with the full-scale cold bending experiments.
3. The stress-strain relationship had no obvious effects on the strain distribution due to cold bending; the cold bending process was a displacement-dominant deformation.
4. At the bending angle of 1 degree, the maximum compressive residual strain was approx. 1.3%. The reduction in the longitudinal yield stress due to the Bauschinger effect was 6% and 27% for Pipes A and B, respectively. The Bauschinger effect was more predominant for the higher strength (grade) and higher Y/T Pipe B than Pipe A.
5. At the bending angle of 1 degree, the ranges of the compressive residual strain over 0.2% were almost equal to the outer diameter of each pipe.

Acknowledgments

The authors wish to thank Prof. Masao Toyoda of Osaka University and Prof. Rudi. M. Denys of Universiteit Gent for their valuable advice, NKK Corporation for the full-scale bending experiments, Ms. Kimiko Keduka of Japan Open Systems Corporation for providing assistance with the analyses, Mr. Shin Uchiki of Tokyo Rigaku Inspection Co., Ltd., for his technical assistance in the tensile tests, and Mr. Naoto Hagiwara and Mr. Koji Yoshizaki of Tokyo Gas Co., Ltd., for their helpful discussion.

References

[1] Abel, A., 1987, "Historical Perspectives and some of the Main Features of the Bauschinger Effect," Materials Forum, **10**(1), pp. 11–26.
[2] Wilkie, S. A., Doblanko, R. M., and Fladager, S. J., 2000, "Case History of Local Wrinkling of a Pipeline," *2000 International Pipeline Conference*, Vol. 2, pp. 917–922.
[3] Das S., Cheng, J. J. R., Murray, D. W., and Wilkie, S. A., 2000, "Laboratory Study of Local Buckling, Wrinkle Development, and Strains for NPS12 Linepipe," *2000 International Pipeline Conference*, Vol. 2, pp. 909–915.
[4] Kobayashi, M., Ando, H., and Oguchi, N., 1995, "Dependence of Longitudinal Subgrade Reaction to Buried Pipe on Displacement Velocities and Cycles of the Ground," *6th U.S.-Japan Workshop on Earthquake Disaster Prevention for Lifeline Systems*, Technical Memorandum of PWRI, No. 3415, pp. 91–106.
[5] Japan Gas Association, 2000, *Recommended Practice for Earthquake Resistant Design of High Pressure Gas Pipeline (in Japanese)*, Tokyo, Japan.
[6] Palynchuk, A., 1983, "Strains Caused by Field Bending of 42-inch Pipe," Pipe Line Industry, March, 23–26.
[7] Bilston, P., and Murray, N., 1993, "The Role of Cold Field Bending in Pipeline Construction," *8th Symposium on Line Pipe Research*, American Gas Association, No. 27, pp. 1–19.
[8] American Petroleum Institute (API), 2000, "Specification for Line Pipe," API SPEC 5L.
[9] Japanese Industrial Standard (JIS), 1998, "Test Pieces for Tensile Test for Metallic Materials," JIS Z 2201.
[10] Hibbit, Karlsson & Sorensen Inc., 1998, *ABAQUS/Standard User's Manual, Version 5.8*, Vol. 2, USA.